Faraday Discussions

Accepted Manuscript

This manuscript will be presented and discussed at a forthcoming Faraday Discussion meeting. All delegates can contribute to the discussion which will be included in the final volume.

Register now to attend! Full details of all upcoming meetings: http://rsc.li/fd-upcoming-meetings

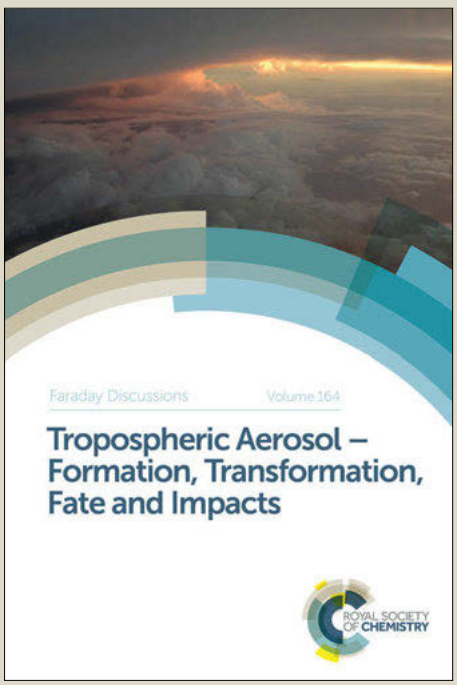

This is an *Accepted Manuscript*, which has been through the Royal Society of Chemistry peer review process and has been accepted for publication.

Accepted Manuscripts are published online shortly after acceptance, before technical editing, formatting and proof reading. Using this free service, authors can make their results available to the community, in citable form, before we publish the edited article. We will replace this *Accepted Manuscript* with the edited and formatted *Advance Article* as soon as it is available.

You can find more information about *Accepted Manuscripts* in the Information for Authors.

Please note that technical editing may introduce minor changes to the text and/or graphics, which may alter content. The journal's standard Terms & Conditions and the Ethical guidelines still apply. In no event shall the Royal Society of Chemistry be held responsible for any errors or omissions in this *Accepted Manuscript* or any consequences arising from the use of any information it contains.

ROYAL SOCIETY OF CHEMISTRY

www.rsc.org/faraday_d

In situ Raman study of lithium-ion intercalation into microcrystalline graphite

Christopher Sole, Nicholas E. Drewett and Laurence J. Hardwick*
DOI: 10.1039/b000000x [DO NOT ALTER/DELETE THIS TEXT]

The first and second order Raman spectra of graphite during the first lithiation and delithiation have been investigated in a typical lithium-ion battery electrolyte. *In situ*, real-time Raman measurements under potential control enable the probing of the graphitic negative electrode surface region during ion insertion and extraction. The experimental results reveal the staging formation of a single particle within a free standing graphitic electrode. In particular, the *in situ* behaviour of the double resonance 2D band during lithiation and delithiation of graphitic carbon has not been previously reported. The 2D band was observed to shift from 2681 to 2611 cm^{-1} and band shape transform into a single Lorentzian from 0.24 to 0.15 V vs. Li/Li^+, providing further information on the electronic structure and C-C bonding of stage 3 and 4 graphite intercalation compounds. The behaviour of the 2D band is in keeping with the Damous-Hérold model of electrochemically derived intercalation, where the graphene layers are flexible and deform around domains of intercalating lithium ions.

1 Introduction

Currently, the major challenge in lithium battery research is to develop systems with even greater power and energy densities[1-4]. Improvements to battery properties will not only depend on the discovery of new materials, but also advances in the understanding of the surface and interfacial region of battery electrodes. Therefore gaining insight into the structure and chemical nature of these interfaces is of major importance.

Investigations into electrode reactions are considerably improved when electrode/solution interface spectra may be recorded as the electrochemical response is obtained. *In situ* Raman spectroscopy is a convenient and non-destructive tool for studying lithiation/delithiation processes within numerous battery electrodes, and it has been utilised to characterise a number of insertion materials over the past couple of decades that are summarised by two recent review articles[5, 6].

Highly crystalline graphitic materials are routinely used as the negative electrode in lithium-ion batteries. Their positive features include a high, reversible specific charge of up to the theoretical value of 372 Ah kg^{-1} (of carbon) for the formation of the donor graphite intercalation compound (GIC) LiC_6, a good cycling stability (for portable electronic applications), a high electronic conductivity and low cost. However, problems persist with insufficient rate performance and electrode degradation over time. In addition, due to the low potential of intercalation (< 0.2 V vs. Li/Li^+) lithium plating is a major safety risk at high charge rates.

The staging process of lithium intercalation into carbon was observed in a typical Li-ion battery electrolyte by Inaba et al.[7] during their pioneering *in situ* Raman microscopy studies. They observed that lithium intercalation proceeds through a

series of staged graphite intercalation compounds (GICs), classified by a stage index, *n*, which represents the number of graphene layers separating layers of intercalated ions. The Raman spectra for GICs with stage $n > 2$ are known to exhibit a doublet G band. The lower (E_{2g2}(i)) and upper (E_{2g2}(b)) frequency components are correspondingly associated with carbon-atom vibrations in interior graphite layers (not adjacent to intercalate layer planes) and in bounding graphite layers (adjacent to intercalate planes). The split in E_{2g2} mode upon intercalation occurs primarily from changes in symmetry at the boundary layer and secondarily from electronic effects of the intercalate molecule. The E_{2g2}(i) band disappears for stage 1 and 2, where no graphite interior layer exists.

A quantitative measure of the intercalation stage index, *n* can be derived from the relative intensities of the Raman doublet, *R* by the following equation[8]:

$$R = \frac{I_i}{I_b} = \frac{\sigma_i}{\sigma_b}\,\frac{n-2}{2} \quad (n > 2) \qquad (1)$$

Where I_i and I_b represent the intensities of the interior E_{2g2}(i) and bounding E_{2g2}(b) layer modes respectively, and $\sigma_i/\ \sigma_b$ is the ratio of the cross section for Raman scattering from the interior and bounding layers (a stage independent constant), which in the case of lithium intercalation is equal to 1.

The staging process during lithium insertion into graphitic carbons had been previously proposed by Dahn et al.[9] following detailed *in situ* powder X-ray diffraction (PXRD) studies. However, whilst PXRD probes the bulk electrode, Raman microscopy offers the ability to follow the processes of lithiation in individual carbon particles, or different areas of a single particle within the electrode[10-12].

Improved understanding of electrochemical processes in functioning battery electrodes will require an insight into more localised lithiation mechanisms. Thus a combination of surface and bulk characterisation is critical in realising the function of these materials under operating battery conditions.

Despite numerous *in situ* Raman studies of Li insertion into carbon[7, 10-20], the effect on the 2D band has yet to be reported. The 2D band is the overtone of the D band. Whilst the D band requires the presence of defects for activation, the overtone originates from a process whereby momentum can always be conserved by two phonons with opposite wave vectors[21], hence the 2D band is always present. The 2D band (also referred to as the G' within the literature) has been used extensively in the research of sp^2 carbons. It allows determination of the number and orientation of graphene layers in few layered graphene samples (1 – 5 layers)[21], in addition to providing information on induced strain[22-24] and charging/doping effects[25, 26]. In this study we report on the behaviour of the 2D band during lithiation into microcrystalline graphite in order to improve our understanding of both the model of Li^+ intercalation and the electronic structure of GICs during lithium intercalation and extraction.

2 Experimental

2.1 Free-standing Electrode Film Preparation

Synthetic microcrystalline graphite (6 μm average particle size), Poly(vinylidene fluoride-hexafluoropropylene) co-polymeric binder (Kynar-flex,

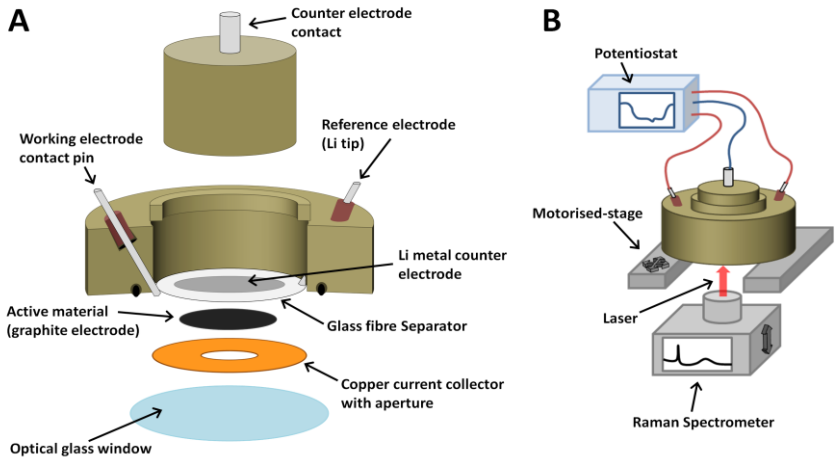

Fig. 1 (A) Schematic of Raman cell assembly; (B) Schematic of Raman cell in operation.

Arkema) and dibutyl phthalate (Aldrich) were dispersed in acetone and then cast onto glass at a thickness of 60 μm. Once dry, the free-standing film was removed from the glass plate with the dibutyl phthalate plasticiser extracted using diethyl ether, leaving a porous film ca. 50 μm thick, which was cut into 6 mm diameter electrodes. These were dried under vacuum at 90^0C, weighed and then transferred to an argon filled glovebox (O_2, H_2O < 1ppm) for Raman cell assembly. The loadings of the electrodes were 5 mg cm^{-2}, with a typical electrode mass being ca. 1.5 mg.

2.2 *In situ* Raman Cell

The electrodes were used as active material within an *in situ* Raman cell (ECC-Opto-Std, El-Cell) configured as shown in Figure 1, and similar to cells used in previous studies[12, 27]. The cell is sealed to atmosphere, enabling non-aqueous electrochemical processes to be investigated *in situ*. The aperture allows a Raman laser to be focussed upon the electrode's back surface during electrochemical cycling, so that Raman spectra may be obtained as a function of potential. The 3 electrode configuration was prepared by placing a small piece of Li metal at the tip of the reference electrode contact pin. Once the cell was sealed, a negative pressure was applied with an electrolyte-filled syringe in order to wet the separator with 1 M $LiPF_6$ in EC-DMC electrolyte (BASF). The Raman cell was then hermetically sealed and removed from the glovebox, whereupon it was positioned atop the Raman microscope stage and connected to a potentiostat.

2.3 Raman Spectroscopy

Raman spectra were recorded with a Raman microscope (Renishaw *inVia*), using a 633nm wavelength laser focussed through an inverted microscope (Leica), via a 50x objective (Leica). The cell had an open circuit potential ca. 3.0 V (all quoted potentials are vs. Li/Li^+) and was galvanostatically cycled at 20 mAg^{-1} carbon (equivalent to a C-rate of C/19, where 1C = charge required to fully lithiate graphite to LiC_6 in 1 hour) between 5 mV and 1.5 V using a potentiostat (Biologic). Suitable

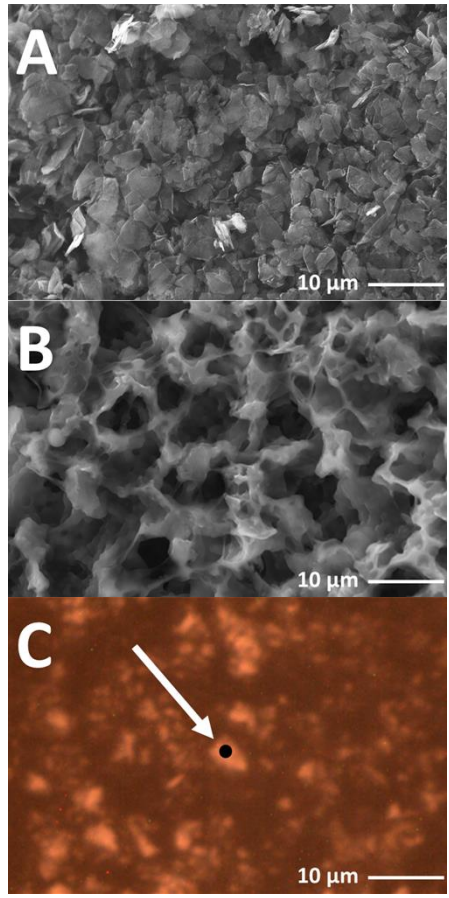

Fig. 2 (A) SEM image of the microcrystalline graphite powder, (B) SEM image of the free-standing electrode cast (C) Optical microscope image of microcrystalline graphite particle from Raman cell working electrode, black spot indicates measured graphite particle

filters were used to minimise the laser power at the surface to < 1 mW cm^{-2}. Higher laser powers should be avoided so as to prevent both heating of the sample area and laser degradation of the surrounding electrolyte (which produces fluorescing species).

2.4 Scanning Electron Microscopy

The synthetic microcrystalline graphite particle and electrode film morphology was characterised using a JEOL 6610 scanning electron microscope operating at an accelerating voltage of 20.0 keV.

3 Results and discussion

A SEM image of the microcrystalline graphite is displayed in Figure 2(A), showing that a distribution of ca. 6 µm sized platelet graphitic particles is present. The free standing electrode cast used for the *in situ* experiments is shown in Figure 2(B), which displays the porosity generated with the film from the DBP extraction.

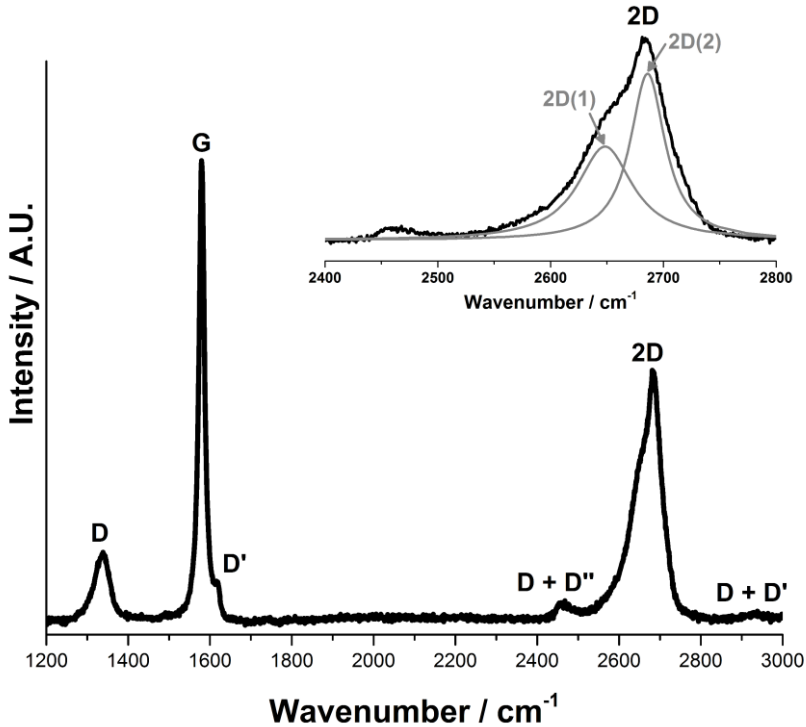

Fig. 3 Raman spectra of 6 μm graphitic carbon. The D, G and 2D bands are observed at 1336 cm^{-1}, 1580 cm^{-1} and 2670 cm^{-1} respectively. The 2D band can be peak fitted to give a sharp peak at 2686 cm^{-1} and a broad shoulder at 2649 cm^{-1} labelled 2D(2) and 2D(1) respectively .

In order to acquire spectra with good signal to noise ratio, the laser was focussed onto a suitable graphite particle as shown in Figure 2(C), and the scattered light was collected from a volume of ca. 1-2 μm^3. The point for *in situ* measurements is carefully designated. On certain areas of the graphite electrode there is minimal detection of Raman peaks from the electrolyte. Furthermore, to allow for the refocussing of the laser throughout the experiment, and checking that the selected measurement spot has been maintained, a particle or area of the electrode with distinguishable features must be selected.

Figure 3 shows the first and second order Raman spectrum for the pristine synthetic graphitic carbon measured in this study. The main peaks observed are the D, G and 2D bands, appearing at 1336 cm^{-1}, 1580 cm^{-1} and ca. 2670 cm^{-1} respectively. The 1580 cm^{-1} peak (E_{2g2}), called the G band after crystalline graphite, is the only easily accessible Raman active mode of the infinite lattice. There is a second Raman active mode E_{2g1} at (41cm^{-1}), but is difficult to observe due to its proximity to the Rayleigh line. The G mode is due to the relative motion of sp^2 carbon atoms in rings as well as chains. The peak at 1336 cm^{-1} is named the D band, from disordered graphite, and can be attributed to the breathing motion of sp^2 atoms in rings at edge planes and defects in the graphene sheet. The origin of the D band has been discussed by Ferrari et al.[21].

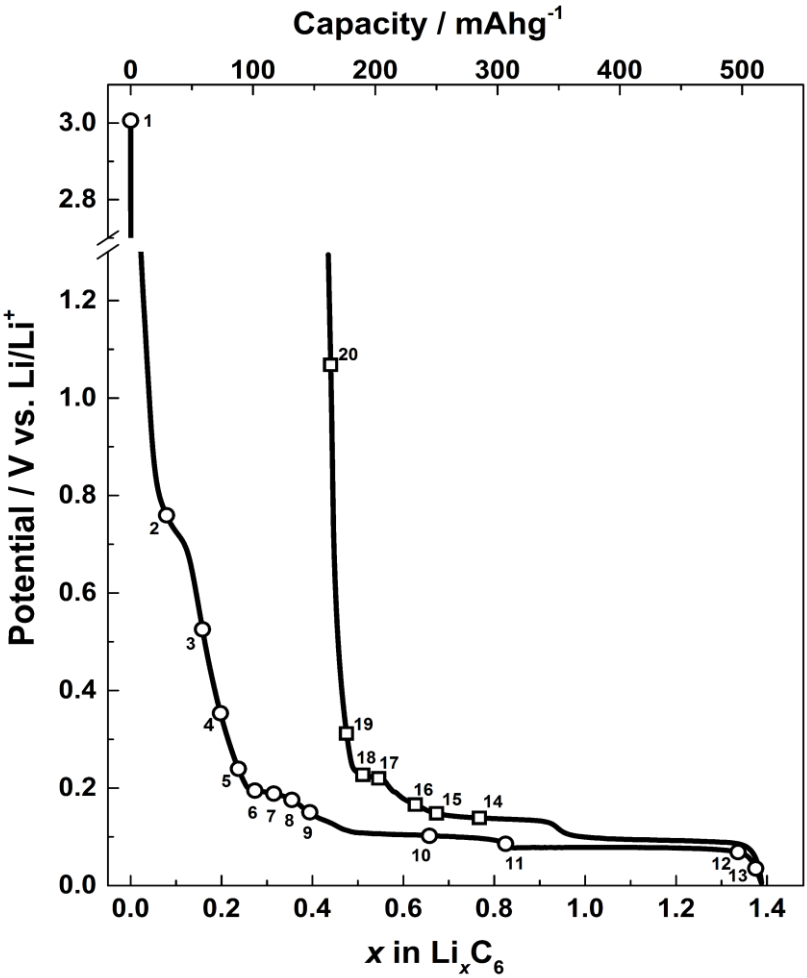

Fig. 4 Graph shows discharge and charge profiles for microcrystalline graphite electrode in the *in situ* Raman cell against metallic lithium counter/ reference. Raman spectra acquisitions are marked with corresponding numbers (as shown in Figure 5).

Peak-fitting of the 2D band gives two peaks in accordance with the literature[28, 29] that have been designated 2D(1) and 2D(2), at 2649 cm^{-1} and 2686 cm^{-1} respectively. It should be noted that Cançado et al.[30] have proposed that the two-peak shape of the 2D band in bulk graphite actually arises from the convolution of an infinite number of peaks.

The load curve showing the first discharge and charge profile is shown in Figure 4. As with other graphitic materials, the charge consumed for the formation of LiC_6 in the first cycle exceeds the theoretical maximum of 372 Ah kg^{-1}. This is due to the partial reduction of electrolyte during the formation of a passivation film called the solid electrode interphase (SEI). The electrochemical performance of the *in situ* Raman cell matches the performance of similar graphitic materials previously reported in the literature[31].

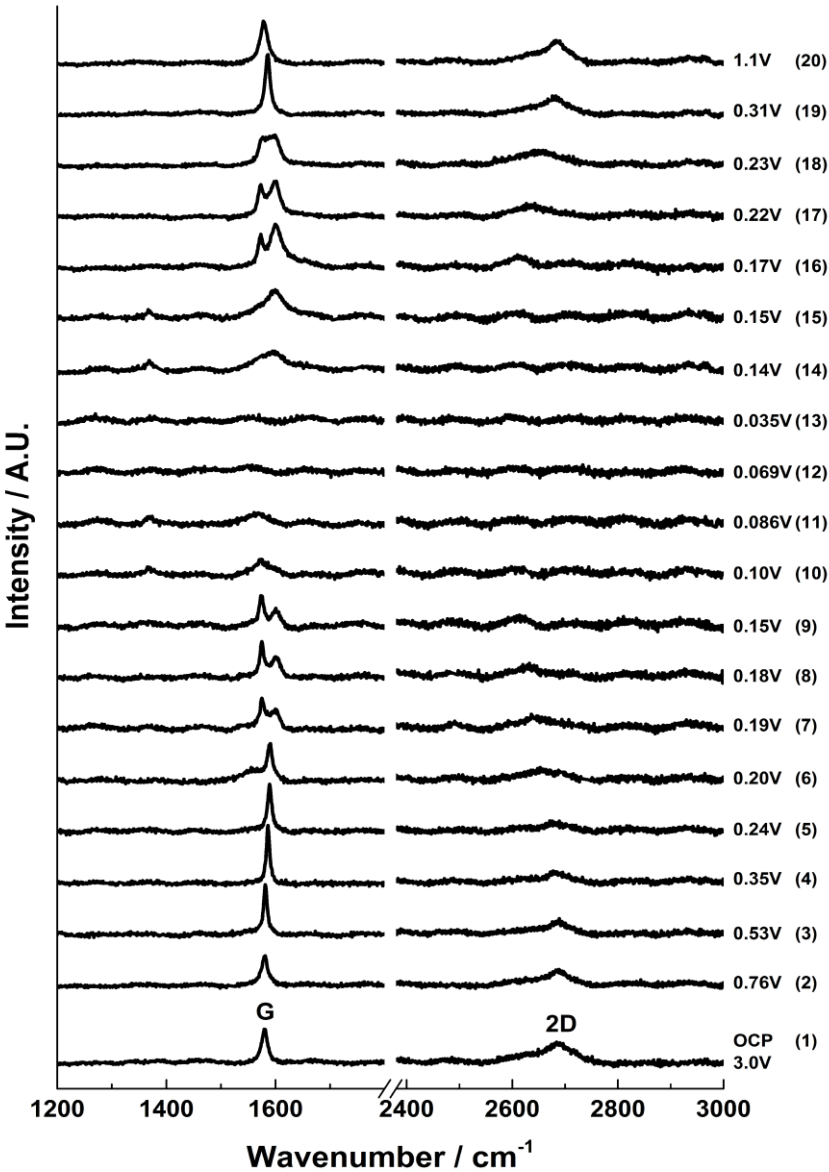

Fig. 5 *In situ* Raman spectral series for the first lithium insertion and extraction into 6 μm graphitic carbon, the potential at each spectral acquisition is labelled to the right.

The results from the first lithium intercalation and de-intercalation cycle are shown in Figure 5. The first order *in situ* Raman spectra compare well to the reported literature[7, 12, 16]. The potential (V) at which each spectrum was collected is displayed. All the spectra are base-line corrected and stacked arbitrarily up the y-axis to allow for clear visualisation. Bands due to the electrolyte are either not detected or negligible because of the employed confocal set-up, which allows a confocal resolution of (1 - 2 μm)[3].

At open circuit potential (ca. 3.0 V vs. Li/Li^+), three main bands are observed in the region between 1000 - 3000 cm^{-1}: the G band at 1580 cm^{-1} and the 2D band at 2670 cm^{-1}. A weak D band is noted at 1330 cm^{-1}.

During lithiation, the first and second order band series of spectra may be divided into four stages of specific interest: the initial loss of D band intensity between potentials ca. 3.0 – 0.6 V; blue-shifting of the G band from 1580 cm^{-1} to 1590 cm^{-1}, accompanied by the gradual weakening (and eventual disappearance) of the 2D(1) band intensity between ca. 0.6 - 0.2 V; splitting of the G band into E_{2g2}(i) (1575 cm^{-1}) and E_{2g2}(b) (1601 cm^{-1}) bands ca. 0.20 - 0.15 V, along with a major red-shift of the 2D(2) band; and finally the appearance of a weak peak around 1370 cm^{-1} and gradual loss of all distinct Raman peaks below ca. 0.10 V associated with the formation of highly conductive, low stage number GICs.

The reverse spectral series (lithium de-intercalation) may also be split into four stages of specific interest: the weak band at 1370 cm^{-1} reappears from ca. 0.14 V along with a broad G band at 1592 cm^{-1}; a weakening of the 1370 cm^{-1} band accompanies the growth, sharpening and blue-shift of the G band from 1592 to 1598 cm^{-1} to form E_{2g2}(b) of stage 2 GIC at ca. 0.15V; the return of the G band doublet, E_{2g2}(i) (1573cm^{-1}) and E_{2g2}(b) (1601 cm^{-1}), as well as the returning 2D(2) band between ca. 0.17 - 0.22 V; and eventually, the reappearance of a sharp singlet G band at 1586 cm^{-1} and the 2D(1) band, and subsequent band shifting back to original OCP band positions between ca. 0.3 - 1.5 V.

Loss of D band

During the galvanostatic first lithium intercalation, the first change observed in the Raman spectrum is the weakening and broadening of the D band. The spot measured in this graphitic material was highly ordered, resulting in a weak D band, which was consequently difficult to observe *in situ*. The loss of intensity of the D band is generally first observed to occur below 1.0 V[12], which coincides with the formation of SEI layer. It steadily decreases with potential until the band is lost into the signal noise below 0.6 V.

Shift and sharpening of G Band

The position of the G band is observed to shift from 1580 cm^{-1} to 1590 cm^{-1}. The frequency shift can be attributed to the increase of the force constants of the in-plane C-C bonds of the dilute stage 1 GICs. Within the region 0.6 - 0.2 V the G band shifted linearly with potential slope of -28±1 cm^{-1} V^{-1} (Figure 6) which is close to the value of -29 cm^{-1} V^{-1} determined by Shi et al.[32] for graphite KS44. The peak shape first narrows and then widens over the potential range (Table 1). The narrowing and shift of the G band both begin below a potential of 0.6 V. This can be attributed to the beginning of lithium insertion at ca. 0.55 V[14]. The dilute stage 1 continues until 0.2 V, below which the formation of low stage number compounds begins. This causes the broadening of the G band as it also consists of weak signals from the emerging E_{2g2}(i) (1575 cm^{-1}) and E_{2g2}(b) (1601 cm^{-1}) bands.

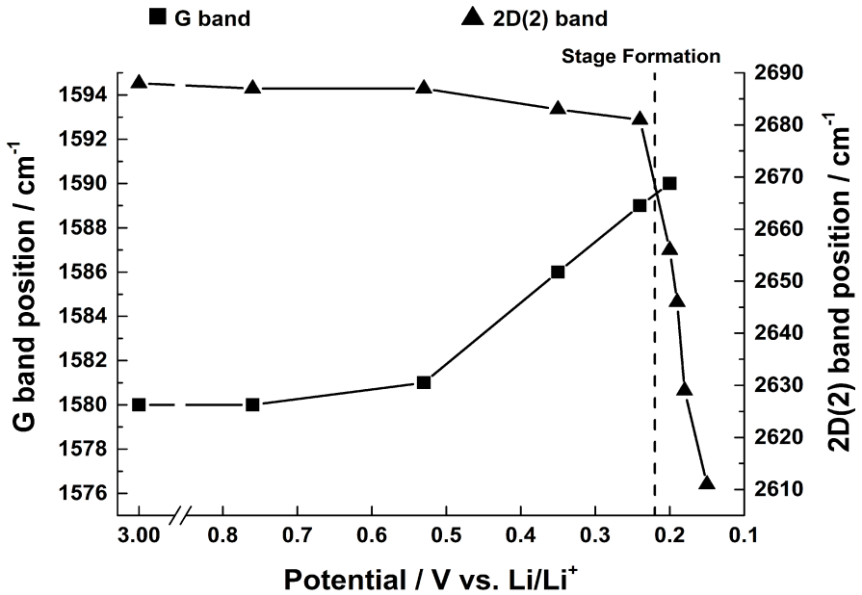

Fig. 6 The shift in G band and 2D(2) position within potential range 3.0 - 0.15 V vs. Li/Li^+ for the first lithiation of graphite. Within the region 0.53 - 0.20 V the G band shifted linearly with potential (slope -27 cm^{-1} V^{-1}). Within the region 0.24 - 0.15 V the 2D(2) band also shifted linearly with potential (slope 802 cm^{-1} V^{-1}).

Shift and shape change of 2D band

The *in situ* behaviour of the double resonance 2D band during lithiation and delithiation of graphitic carbon in a typical Li-ion battery electrolyte has not been previously reported. In contrast to the D band, which is widely reported to lose signal intensity between ca. 1 - 0.6 V[12], the 2D band remains visible until below ca. 0.15 V, when the high conductivity of low stage number GICs makes band observation difficult. As mentioned previously, no defects are required for activation of the 2D band and so it may be proposed that, whilst surface passivation/lithiation of defects may lead to the weakening and eventual disappearance of the D band, the 2D band remains visible. The 2D band position remains fairly constant until 0.53 V, including during the formation of the solid electrolyte interphase (below 1.0 V). Between 0.53 V and 0.24 V there is a gradual red-shift of the 2D(2) peak position of 21±1 cm^{-1} V^{-1} accompanying the formation of dilute stage 1 GIC signalled by the blue-shift of the G band. Between these potentials the fitted 2D(1) peak intensity falls, making fitting difficult (due to the high background) and causing some uncertainty in the assigned position. Below 0.24 V the 2D(1) peak is no longer discernible.

Table 1 In situ Raman peak positions and full width at half maximum (FWHM) of first electrochemical lithium insertion and extraction into microcrystalline graphite

E(V)	G		E_{2g2}(i)		E_{2g2}(b)		2D(1)		2D(2)	
	ω (cm^{-1})	FWHM (cm^{-1})	ω (cm^{-1})	FWHM (cm^{-1})	ω (cm^{-1})	FWHM (cm^{-1})	ω (cm^{-1})	FWHM (cm^{-1})	ω (cm^{-1})	FWHM (cm^{-1})
3.00	1580	12	-	-	-	-	2625	61	2688	53
0.76	1580	14	-	-	-	-	2625	57	2687	50
0.53	1581	9	-	-	-	-	2632	68	2687	36
0.35	1586	7	-	-	-	-	2622	30	2683	35
0.24	1589	9	-	-	-	-	2615	27	2681	45
0.2	1590	11	-	-	-	-	-	-	2656	75
0.19	-	-	1576	12	1599	15	-	-	2646	73
0.18	-	-	1575	9	1600	15	-	-	2629	59
0.15	-	-	1574	11	1601	15	-	-	2611	31
0.1	-	-	-	-	-	-	-	-	-	-
0.086	-	-	-	-	-	-	-	-	-	-
0.069	-	-	-	-	-	-	-	-	-	-
0.035	-	-	-	-	-	-	-	-	-	-
0.14	-	-	-	-	1592	57	-	-	-	-
0.15	-	-	-	-	1598	44	-	-	-	-
0.17	-	-	1573	8	1601	30	-	-	2614	51
0.22	-	-	1573	11	1598	22	-	-	2636	73
0.23	-	-	1577	16	1597	23	-	-	2649	90
0.31	1586	11	-	-	-	-	2630	48	2682	45
1.1	1579	15	-	-	-	-	2635	60	2685	39

At ca. 0.20 V, accompanying the onset of stage 4 GIC formation, the gradient of the 2D(2) peak red-shift increases significantly to a rate of 802±87 cm^{-1} V^{-1} (Figure 6, Table 1). A similar red-shift in the 2D position has been previously observed during the n type doping of, and the intercalation of other metal ions into GICs[24, 26]. This shift may be attributed to electronic doping and increased in-plane (biaxial) lattice strain accompanying Li^+ insertion. The linear nature of this shift between 0.24 - 0.15 V, and the biaxial nature of the attributed lattice strain, implies that the graphene layers in the graphitic carbon are becoming increasingly distorted on lithium intercalation. This is in keeping with the Damous-Hérold model of intercalation, where the graphene layers are flexible and deform around the intercalating lithium ions, and contrary to the Rüdorff, which proposes a sequential filling up of alternating graphene interlayer spaces with no structural distortions induced within the individual graphene sheets as seen in Figure 7.

The apparent shape change of the 2D band towards a single Lorentzian peak suggests the graphene layers in the stage 4 GIC have become electronically similar to single layer graphene, most likely due to electronic decoupling resulting from the transfer of charge from the electron from the external circuit to the bounding layers[24]. The 2D band is no longer observable below 0.10 V. This suggests that stage 2 and stage 1 GIC are not visible in the Raman spectra as all graphene layers of the GIC are charged, and thus no longer give a Raman signal.

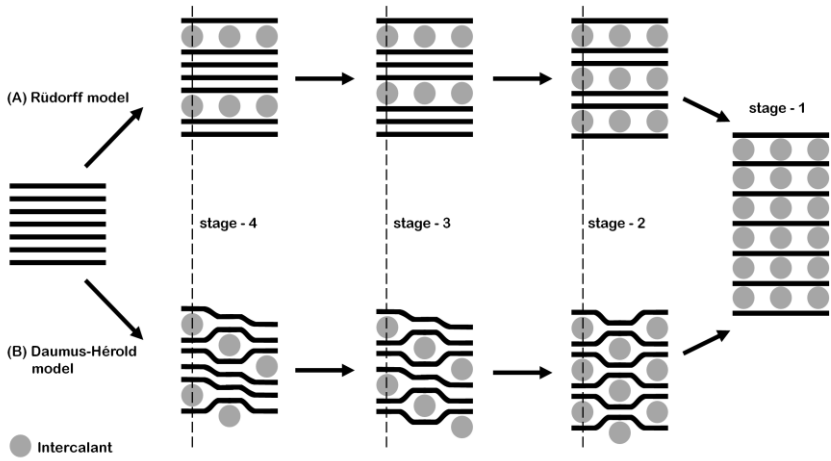

Fig. 7 Schematic of (A) Rüdorff and (B) Daumus-Hérold models of ion intercalation into graphite

Splitting of the G band

As the potential continues decreasing below 0.20 V the G band continues to broaden, with two side bands beginning to grow and become distinct bands. These peaks can be assigned to the intensities of the interior E_{2g2}(i) (1575 cm^{-1}) and bounding E_{2g2}(b) (1601 cm^{-1}) bands. These two bands quickly become prominent at the detriment of the dilute stage 1 band. This transformation points towards a phase transition from the dilute stage 1 to a staged phase with n > 2. Using equation (1)[7] and the intensities of the bands from the peak fitting, the ratio R is calculated to be ca. 1.0, which signifies the establishment of a stage 4 lithium GIC (graphite intercalation compound) at 0.19 V (spectrum number 7).

The phase transition is related to the change from a random distribution of lithium ions into a more compact distribution in the staged compound. The shift of the E_{2g2}(b) band to 1601 cm^{-1} is due to the further increase of the C-C bond force constants.

Formation of Stage 2 GIC

The reduction and eventual disappearance of the E_{2g2}(i) band is observed between 0.10 V and 0.069 V. However, the E_{2g2}(b) band at 1601 cm^{-1} is also seen to disappear. Based on past reports of stage 2 GIC materials that have been produced from chemical synthesis, it is expected that the Raman spectrum should display a single band at ca. 1601 cm^{-1} [33]. This is clearly not the case and instead a broad band at 1550 cm^{-1} is seen. This is tentatively assigned as the blue-shifted E_{2g2}(b) of a stage 2 liquid GIC, where there is no longer ordered distribution of lithium within the planes. However, a recent article by Zabel et al.[34] on graphene sheets under strain shows a similar G-band shift for graphene sheets under ca. 1 bar of pressure, perhaps as a result of contortion of graphene sheets seen from the Daumaus-Hérold model of intercalation.

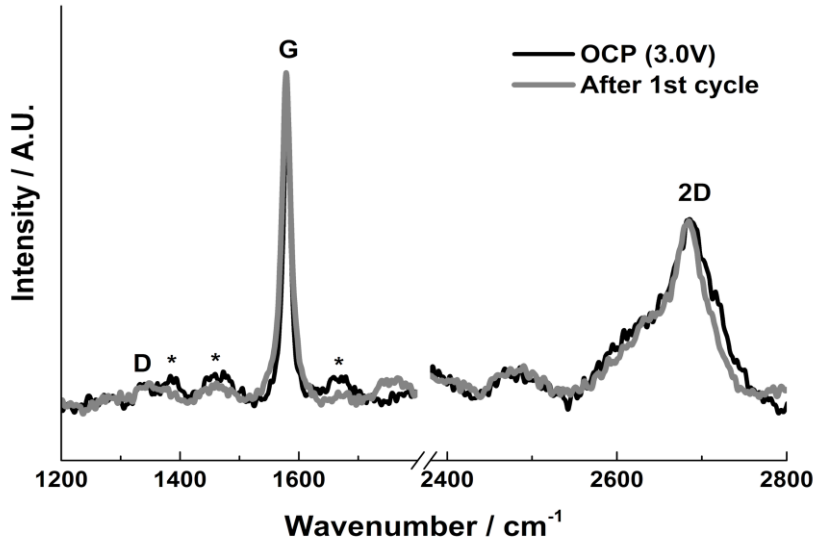

Fig. 8 *In situ* Raman spectra before and after lithiation,* indicates signal from electrolyte bands.

This shift can then be explained by charge transfer effects during intercalation of a donor species where electrons occupy the π* orbital and thus weaken the C-C bond strength. Such an effect has been seen for the intercalation of donor species into less ordered carbon materials.[13, 35, 36] This broad band continues to blue-shift and broadens until it disappears into the noise at ca. 1540 cm^{-1}. Raman bands are thought to be no longer visible because of the increase of electrical conductivity of these low stage GICs, which leads to a reduction in optical skin depth, and results in a low Raman scattering intensity[7].

First de-lithiation

During the first de-lithiation, the reverse trend for the Raman spectra is seen as shown in Figure 5, as the potential is increased from 0.005 to 1.5 V. At 0.14 V two bands are observed at 1370 cm^{-1} and 1592 cm^{-1}. The band at 1592 cm^{-1} is seen to shift and grow in intensity to 1601 cm^{-1} as the potential is increased. This indicates the formation of the E_{2g2}(b) and thus the formation of a pure stage 2 GIC. The 1370 cm^{-1} band is absent by 0.17 V. At 0.17 V a second peak emerges at 1573 cm^{-1}, the E_{2g2}(i), which grows at the expense of the E_{2g2}(b). This marks the return to a stage 3 GIC and then to a stage 4 by ca. 0.17 V.

From 0.22 to 0.24 V there is a mixture of stage 4 and dilute stage 1 and the doublet G band returns again to the single E_{2g2} at 1586 cm^{-1}, which then blue-shifts back to 1579 cm^{-1}, showing the passage from dilute stage 1 to fully de-intercalated graphite. The shift in G band position is shown clearly between 0.31 – 1.1 V vs. Li/Li^+.

The Raman spectra before and after lithiation is shown in Figure 8. Both show very similar features, and the relative intensites of the G and 2D bands remain the same. Both spectra display a weak D band, indicating that the area measured did not become further disordered during the first Li^+ insertion/extraction cycle. The lack of change of the spectra represents indicates that the measured graphite particle has

experienced no significant structural change.

The reappearance of the 2D band is discernible at 0.17 V at 2614 cm^{-1} with a single Lorentzian fit that we have ascribed to the returning 2D(2) peak. This is a similar position to the last observable position during lithiation (2611cm^{-1} at 0.15V) suggesting the return of the stage 3 GIC. The 2D(2) peak red-shifts and broadens between ca. 0.17 V to 0.23 V until the eventual reforming of the low energy 2D(1) peak at 0.31 V. This splitting of the 2D band marks the renewed electronic coupling between graphene layers and suggests the formation of the dilute stage 1 GIC. Both 2D(1) and 2D(2) peaks shift back towards their OCP positions.

4 Summary and Conclusions

Graphitic carbon remains the dominant active material used within lithium-ion negative electrodes. Understanding the mechanics of Li^+ intercalation into actual practical graphitic anodes is important in optimising this material in terms of performance, lifetime and safety. *In situ* Raman spectrum of the first electrochemical lithiation and de-lithiation cycle on a single point on a graphite electrode were obtained with good signal to noise ratio and minimal detection of electrolyte bands.

The obtained first order spectra agree with previous reports in particular with observation of the G-band splitting, indicating the formation of a staged GIC. The behaviour of the second order *in situ* Raman spectra was reported for the first time during the first lithium insertion and extraction cycle. The 2D band was observed to shift to lower wavenumbers (2681 to 2611 cm^{-1}) when stage 4 and 3 graphite intercalation compounds were formed. The shift of the 2D band supports the Damous-Hérold model of electrochemically derived intercalation, where the graphene layers are flexible and deform around domains of ordered intercalated lithium ions. The opposite trends were observed in the Raman spectra during lithium extraction indicating the lithium is removed in a reversible manner, with comparable initial and final spectra. This demonstrates that, on this particular point of the graphite electrode, no disordering of the structure resulted from a single cycle of lithium insertion and extraction.

Acknowledgements

We gratefully acknowledge the EPRSC for the funding of this research under grant number EP/K016954/1.

[a] *Stephenson Institute for Renewable Energy, Department of Chemistry, University of Liverpool, UK, L69 7ZF*
** Corresponding author. Email: laurence.hardwick@liv.ac.uk*

References

1. A. S. Aricò, P. Bruce, B. Scrosati, J.-M. Tarascon and W. V. Schalkwijk, *Nat. Mater.*, 2005, **4**, 366.
2. P. G. Bruce, B. Scrosati and J.-M. Tarascon, *Angew. Chem. Int. Ed.*, 2008, **47**, 2930.
3. P. G. Bruce, S. A. Freunberger, L. J. Hardwick and J.-M. Tarascon, *Nat. Mater.*, 2012, **11**, 19.
4. J. B. Goodenough and K.-S. Park, *J. Am. Chem. Soc.*, 2013, **135**, 1167.
5. R. Baddour-Hadjean and J. P. Pereira-Ramos, *Chem Rev*, 2010, **110**, 1278.
6. V. Stancovski and S. Badilescu, *J. Appl. Electrochem.*, 2014, **44**, 23.
7. M. Inaba, H. Yoshida, Z. Ogumi, T. Abe, Y. Mizutani and M. Asano, *J. Electrochem. Soc.*, 1995, **142**, 20.

8. S. A. Solin, *Graphite Intercalation Compounds*, Springer-Verlag, Berlin, 1990.
9. R. Fong, U. Vonsacken and J. R. Dahn, *J. Electrochem. Soc.*, 1990, **137**, 2009.
10. K. Dokko, Q. F. Shi, I. C. Stefan and D. A. Scherson, *J. Phys. Chem. B*, 2003, **107**, 12549.
11. Y. Luo, W. B. Cai and D. A. Scherson, *J. Electrochem. Soc.*, 2002, **149**, A1100.
12. L. J. Hardwick, H. Buqa and P. Novak, *Solid State Ionics*, 2006, **177**, 2801.
13. M. Inaba, H. Yoshida and Z. Ogumi, *J. Electrochem. Soc.*, 1996, **143**, 2572.
14. W. W. Huang and R. Frech, *J. Electrochem. Soc.*, 1998, **145**, 765.
15. J. C. Panitz, F. Joho and P. Novak, *Appl. Spectrosc.*, 1999, **53**, 1188.
16. S. Migge, G. Sandmann, D. Rahner, H. Dietz and W. Plieth, *J. Solid State Electrochem.*, 2005, **9**, 132.
17. P. Novak, D. Goers, L. Hardwick, M. Holzapfel, W. Scheifele, J. Ufhiel and A. Wursig, *J. Power Sources*, 2005, **146**, 15.
18. L. J. Hardwick, H. Buqa, M. Holzapfel, W. Scheifele, F. Krumeich and P. Novak, *Electrochim. Acta*, 2007, **52**, 4884.
19. L. J. Hardwick, P. W. Ruch, M. Hahn, W. Scheifele, R. Kotz and P. Novak, *J. Phys. Chem. Solids*, 2008, **69**, 1232.
20. V. Baranchugov, E. Markevich, G. Salitra, D. Aurbach, G. Semrau and M. A. Schmidt, *J. Electrochem. Soc.*, 2008, **155**, A217.
21. A. C. Ferrari and D. M. Basko, *Nature Nanotech.*, 2013, **8**, 235.
22. T. M. G. Mohiuddin, A. Lombardo, R. R. Nair, A. Bonetti, G. Savini, R. Jalil, N. Bonini, D. M. Basko, C. Galiotis, N. Marzari and Phys. Rev. B 2009, 205433-8 *Phys. Rev. B*, 2009, **79**, 205433.
23. C. Metzger, S. Remi, M. Liu, S. V. Kusminskiy, A. H. Castro Neto, A. K. Swan and B. B. Goldberg, *Nano Lett.*, 2010, **10**, 6.
24. J. C. Chacón-Torres, L. Wirtz and T. Pichler, *ACS Nano*, 2013, **7**, 9249.
25. W. Zhao, P. H. Tan, J. Liu and A. C. Ferrari, *J. Am. Chem. Soc.*, 2011, **133**, 5941.
26. R. Parret, M. Paillet, J.-R. Huntzinger, D. Nakabayashi, T. Michel, A. Tiberj, J.-L. Sauvajol and A. A. Zahab, *ACS Nano*, 2013, **7**, 165.
27. L. J. Hardwick, M. Hahn, P. Ruch, M. Holzapfel, W. Scheifele, H. Buqa, F. Krumeich, P. Novák and R. Kötz, *Electrochim. Acta*, 2006, **52**, 675.
28. J. Nemanich and S. A. Solin, *Phys. Rev. B*, 1979, **20**, 392.
29. R. P. Vidano, O. B. Fischbach, L. J. Willis and T. M. Loehr, *Solid State Commun.*, 1981, **39**, 341.
30. L. G. Cançado, A. Reina, J. Kong and M. S. Dresselhaus, *Phys. Rev. B*, 2008, **77**, 245408
31. H. Buqa, A. Wursig, A. Goers, L. J. Hardwick, M. Holzapfel, P. Novak, F. Krumeich and M. E. Spahr, *J. Power Sources*, 2005, **146**, 134.
32. Q. F. Shi, K. Dokko and D. A. Scherson, *J. Phys. Chem. B*, 2004, **108**, 4789.
33. M. S. Dresselhaus and G. Dresselhaus, *Adv. Phys.*, 2002, **51**, 1.
34. J. Zabel, R. R. Nair, A. Ott, T. Georgiou, A. K. Geim, K. S. Novoselov and C. Casiraghi, *Nano Lett.*, 2012, **12**, 617.
35. M. Endo, C. Kim, T. Karaki, T. Fujino, M. J. Matthews, S. D. M. Brown and M. S. Dresselhaus, *Synth. Met.*, 1998, **98**, 17.
36. Z. X. Wang, X. J. Huang, R. J. Xue and L. Q. Chen, *Carbon*, 1999, **37**, 685.